J. Fluid Mech. (1990), *vol.* 217, *pp.* 143–165
Printed in Great Britain

On the directly generated resonant standing waves in a rectangular tank

By LEV SHEMER

Department of Fluid Mechanics and Heat Transfer, Faculty of Engineering, Tel-Aviv University, Ramat-Aviv, Israel

(Received 22 November 1988 and in revised form 14 December 1989)

A numerical study based on the nonlinear Schrödinger equation, as applied to nonlinear resonant standing waves excited directly by a wavemaker in a rectangular tank, is presented. The stationary solutions of the problem serve as a starting point of the investigation. Bifurcations from a single steady state to multiple stationary solutions are obtained for several values of damping coefficients along the tank and at the wavemaker. The stability of the latter solutions is tested. Limit-cycle or fixed-point solutions are obtained. The results of the numerical study are discussed in connection with experimental data. The necessity of incorporation of dissipation at the wavemaker in the theoretical model in order to obtain qualitative agreement with experiment is demonstrated.

1. Introduction

In recent years there has been considerable interest in standing waves that are excited in the vicinity of the cutoff frequency in a closed container or in a wave tank, both in the case of direct excitation and that of parametric subharmonic resonance. Even in a relatively simple case of direct excitation of waves in a circular cylinder, a rich variety of nonlinear phenomena, such as various types of bifurcations, period doublings and chaotic states were observed (Funakoshi & Inoue 1988). When such waves are excited parametrically, the problem becomes rather complicated, Ciliberto & Gollub (1985), Umeki & Kambe (1989), although it can still be described by a system of ordinary nonlinear differential equations.

In the present work we consider resonant standing gravity waves which are excited in a semi-infinite rectangular tank of width b by a wavemaker located at $x = 0$, having an instantaneous shape with a characteristic length of $L = 2b/n$, n being the mode number. Such waves of the first mode were studied by Barnard, Mahony & Pritchard (1977, hereinafter referred to as BMP). Only steady wave regimes were observed by BMP. In their theoretical analysis they derived the governing ordinary nonlinear differential equation which describes the values of the stationary wave amplitudes along the tank. BMP were the first to realize that incorporation of damping is necessary in order to obtain qualitative agreement between their experimental results and the theoretical predictions. BMP also reported on two different wave patterns that were observed in the tank.

Kit, Shemer & Miloh (1987, hereinafter referred to as KSM), studied resonant waves of the second mode for a wide range of wavemaker amplitudes and frequencies. In contrast to BMP, they observed experimentally both steady and slowly modulated regimes. A range of values of the detuning coefficient λ was found where either steady or modulated (on a long timescale) wave regimes could be observed, depending on

initial conditions. Steady regimes were observed when the forcing frequency was gradually increased (at constant wavemaker amplitude), until a sharp transition to a modulated regime occurred. When the forcing frequency was slowly reduced after this transition, the unsteady pattern could be retained for relatively low frequencies, and a reverse transition to the steady regime occurred at values of λ notably lower than those for which the transition from steady to modulated regime was observed. Similar hysteresis was obtained by slow variation of the forcing amplitude at a constant frequency. Numerical solution of the model nonlinear Schrödinger (NLS) equation derived by KSM gives the various wave patterns observed in the experiment. Qualitative agreement between the experimental results and the numerical predictions of the long-time evolution of the wave amplitude distribution along the tank was obtained by KSM, provided that in addition to the damping term in the governing equation, which accounts for dissipation along the tank, another damping term is introduced in the boundary condition at the wavemaker.

The importance of the dissipation at the wavemaker was substantiated in a later work by Shemer & Kit (1988), where both complex dissipation terms, along the tank and at the wavemaker, were obtained theoretically for the case of purely viscous dissipation mechanism in the Stokes layers at solid walls. In that investigation it was experimentally demonstrated that the wavemaker dissipation affects the long-time evolution pattern of the nonlinear standing resonant waves in a significant way. Specifically, it was shown that the variation of the dissipation rate at the wavemaker by adding roughness elements to the wavemaker surface caused drastic changes in the wave regime in the tank. It was also shown by Shemer & Kit that the incorporation of the wavemaker dissipation in the theoretical model led to good quantitative agreement between the experimental and the numerical results. It should be stressed, however, that for such agreement to be attained, the values of the dissipation coefficients had to be substantially higher than those predicted by a theory based on a purely viscous dissipation mechanism.

The experiments of KSM were performed with the wavemaker equipped with the roughness elements. For a smooth wavemaker, practically no hysteresis in transition between the steady and the modulated regimes was observed. In this case the hysteresis was shifted down to frequencies where only a steady wavefield existed in the tank. Detailed measurements of two different steady wave distributions in the tank were reported by Shemer, Chemesse & Kit (1989).

Miles (1988) rederived the governing NLS equation for directly excited standing waves in a rectangular tank, using a variational formulation. The resulting equation is in agreement with KSM. He has found that under certain conditions the governing equation possesses multiple stationary solutions. This was related by Miles to the two different wave regimes observed in the experiments by BMP.

In the present work the Miles analysis is extended in several directions. First, the dissipation at the wavemaker is incorporated in the Miles equations in §2 and the effects of the wavemaker dissipation are studied in §3. The whole problem is revisited in §4 from an experimental point of view, and bifurcation diagrams are presented which show the domains of unique and multiple solutions in terms of the single variable parameter of the problem, the detuning coefficient λ. The results are presented for a number of dissipation coefficients along the tank and at the wavemaker. Possible stationary distributions of the wave amplitude along the tank are plotted in §5. The next step is made in §6, where the time-dependent NLS equation is employed to study the stability and the long-time evolution of the previously obtained stationary solutions. These numerical experiments yield only

fixed-point or limit-cycle type solutions. A comparison between the numerical solutions and experimental data is performed in §7. Section 8 offers a brief summary and conclusions.

2. Governing equations

Following KSM and Shemer & Kit (1988), we consider a semi-infinite deep rectangular tank with side walls at $y = 0$ and $y = b$ and a wavemaker at $x = 0$. All variables are rendered dimensionless using b as a lengthscale and $(b/g)^{\frac{1}{2}}$ as a timescale. For standing waves of the nth mode, the wave number k_n and the cutoff frequency ω_n are given by

$$k_n = n\pi, \quad \omega_n = k_n^{\frac{1}{2}}. \tag{1}$$

The slow variable along the tank X and the slow time variable T are defined by

$$X = \tfrac{1}{2}(n\pi)^5 \epsilon^2 x, \quad T = \tfrac{1}{4}(n\pi)^3 \epsilon \omega_n t, \tag{2}$$

where the small parameter ϵ represents the amplitude of forcing and is proportional to the dimensionless stroke of the wavemaker at the mean surface level, s. The corresponding coefficient of proportionality depends on the wavemaker shape function, see Shemer & Kit (1988). The ratio of the deviation of the forcing frequency ω from ω_n to the forcing amplitude ϵ is represented by the detuning coefficient λ:

$$\lambda = \frac{4\omega_n(\omega - \omega_n)}{n^4\pi^4\epsilon}. \tag{3}$$

The velocity potential ϕ is related to the complex, normalized amplitude C by

$$\phi = \epsilon^{\frac{1}{2}} \cos(k_n y) \exp(k_n z) [C(X, T) \exp(-\mathrm{i}\omega t) + \text{c.c.}], \tag{4}$$

where c.c. denotes complex conjugate. In the presence of dissipation, the slow space and time variation of the complex amplitude of the velocity potential $C(X, T)$ is governed by the NLS equation

$$\mathrm{i}\frac{\partial C}{\partial T} + \frac{\partial^2 C}{\partial X^2} + (\lambda + \hat{a}_1) C + 2|C|^2 C = 0, \tag{5}$$

with the boundary condition at the wavemaker having the following form:

$$\frac{\partial C}{\partial X} = -\mathrm{i} - \hat{a}_2 C \quad \text{at } X = 0. \tag{6}$$

The amplitude C vanishes as $X \to \infty$. The complex dissipation coefficients along the tank, $\hat{a}_1$, and at the wavemaker, $\hat{a}_2$, can be presented in the case of purely viscous dissipation as

$$\hat{a}_1 = a_1(1 + \mathrm{i}), \quad \hat{a}_2 = a_2(1 + \mathrm{i}). \tag{7}$$

Comparison with the available experimental data indicate that estimates of a_1, and to an even greater extent, of a_2, based on viscous dissipation only are substantially below their actual values, which may vary significantly among various experimental facilities and under different experimental conditions (Kit & Shemer 1989; Shemer *et al.* 1989). The arguments of both complex dissipation coefficients will be assumed to be equal to $\frac{1}{4}\pi$, as in (7). This is in reasonable agreement with the experiments.

Miles (1988) has considered stationary solutions of (5) subject to the boundary condition at the wavemaker (6) corresponding to vanishing dissipation at the

wavemaker, i.e. $a_2 = 0$. A modification of Miles' approach is now presented which takes into account the complex dissipation coefficient along the tank, as well as the dissipation at the wavemaker. In Miles' presentation the governing equation has the following form:

$$\frac{\mathrm{d}^2 A}{\mathrm{d}\xi^2} + (\mathrm{e}^{\mathrm{i}\phi} + |A|^2) A = 0. \tag{8}$$

The relation between the Miles' variables A and ξ and our variables C and X is given by

$$C = A(\tfrac{1}{2}\lambda_1)^{\frac{1}{2}}, \quad X = -\frac{\xi}{\lambda_1^{\frac{1}{2}}}, \tag{9a, b}$$

with

$$\phi = \tan^{-1}\left(\frac{a_1}{\lambda + a_1}\right), \quad \lambda_1 = [(\lambda + a_1)^2 + a_1^2]^{\frac{1}{2}}, \tag{10}$$

λ_1 being the absolute value of the linear term coefficient in (5). The boundary condition at the wavemaker (6) rewritten in terms of Miles' variables is

$$\frac{\mathrm{d}A}{\mathrm{d}\xi} = -\frac{\mathrm{i}\sqrt{2}}{\lambda_1} - a_2 \frac{1+\mathrm{i}}{\lambda_1^{\frac{1}{2}}} A \quad \text{at } \xi = 0. \tag{11}$$

The transformation

$$\frac{\mathrm{d}\log A}{\mathrm{d}\xi} = L + \mathrm{i}K \tag{12}$$

is introduced, where L and K are regarded as functions of Z,

$$Z = \left(\frac{|A|}{A_*}\right)^2, \quad A_* = (2\sin^2\tfrac{1}{2}\phi + \tfrac{1}{2}\cos^2\tfrac{1}{2}\phi)^2. \tag{13}$$

The complex equation (8) is replaced by a system of two real equations:

$$2LZ\frac{\mathrm{d}L}{\mathrm{d}Z} + L^2 - K^2 + \cos^2\tfrac{1}{2}\phi - \sin^2\tfrac{1}{2}\phi + ZA_*^2 = 0, \quad L\frac{\mathrm{d}(ZK)}{\mathrm{d}Z} = -\tfrac{1}{2}\sin\phi. \tag{14a, b}$$

Additional details can be found in Miles (1988). Equating the absolute values and the arguments of the boundary condition at the wavemaker (11) in the presence of wavemaker dissipation yields, respectively,

$$M(Z_0) = \left(\frac{2}{\lambda_1}\right)^{\frac{1}{2}} \tag{15a}$$

and

$$\arg(A) = -\tfrac{1}{2}\pi - \tan^{-1}\frac{(a_2/\lambda_1^{\frac{1}{2}}) + K}{(a_2/\lambda_1^{\frac{1}{2}}) + L}, \quad Z = Z_0, \tag{15b}$$

where

$$M = \left[\left(\frac{a_2}{\lambda_1^{\frac{1}{2}}} + L\right)^2 + \left(\frac{a_2}{\lambda_1^{\frac{1}{2}}} + K\right)^2\right]^{\frac{1}{2}} A_* Z^{\frac{1}{2}}, \tag{16}$$

and Z_0 corresponds to the position of the wavemaker ($\xi = 0$). Equations (14) are integrated starting from infinity, i.e. from the singular point $Z = 0$, so that the dependence $M = M(Z)$ is obtained. Steady solutions correspond to the points $Z = Z_0$ where (15a) is satisfied. Equation (12) can now be integrated to yield

$$\xi = \frac{1}{2}\int_Z^{Z_0} \frac{\mathrm{d}Z}{ZL}, \quad \arg(A) = \arg(A(Z_0)) + \frac{1}{2}\int_{Z_0}^{Z} \frac{K\,\mathrm{d}Z}{ZL}. \tag{17a, b}$$

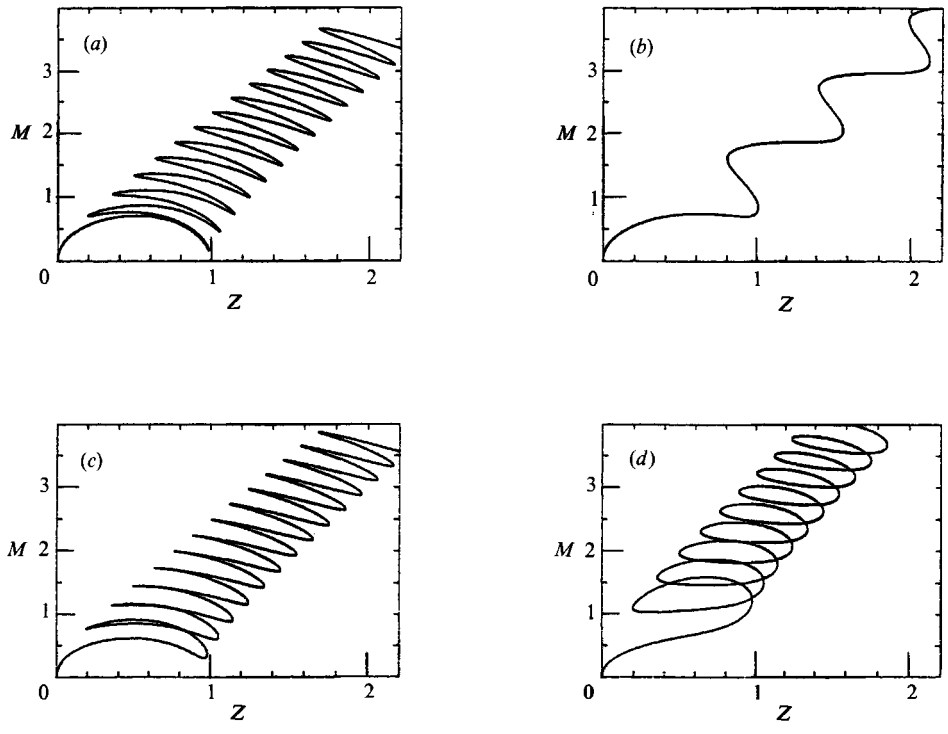

FIGURE 1. The dependence $M(Z)$. (*a*) $\lambda/a_1 = -10.0$, $a_2 = 0$, $\phi = 173.7°$; (*b*) $\lambda/a_1 = -2.5$, $a_2 = 0$, $\phi = 146.3°$; (*c*) $\lambda/a_1 = -10.0$, $a_2/\lambda^{\frac{1}{2}} = 0.1$, $\phi = 173.7°$; (*d*) $\lambda/a_1 = -10.0$, $a_2/\lambda^{\frac{1}{2}} = 0.5$, $\phi = 173.7°$.

Using (9), all possible stationary distributions of complex amplitude $C(X)$ can now be obtained, and their stability can be checked by substituting them into (5) as initial conditions.

3. Effects of dissipation at the wavemaker

We consider first the case of vanishing dissipation at the wavemaker, $a_2 = 0$. The function $M = M(Z)$ then depends on a single parameter ϕ, see (8), (14) and (15). There is a straightforward transformation from ϕ and the parameter in the wavemaker boundary condition (15), λ_1, to the physical variables a_1 and λ, which follows from (10):

$$a_1 = \lambda_1 \tan\phi, \quad \lambda = \lambda_1(\cos\phi - \sin\phi). \tag{18}$$

Thus the argument ϕ is a function of the ratio of the physical parameters, λ/a_1, only.

The dependence of M on Z is shown in figure 1(*a*) for $\lambda/a_1 = -10.0$, $\phi = 173.7°$. Single stationary solutions are obtained only when $M < 0.156$. The domain of M where only one stationary solution exists expands with decreasing ϕ. At smaller angles ϕ, there may be a limited range of M where multiple solutions are possible. In the case of $\phi = 146.3°$, $\lambda/a_1 = -2.5$, presented in figure 1(*b*), multiple stationary solutions exist for $0.702 < M < 0.745$. Stationary wave amplitude distributions become unique for arbitrary M for $\phi < 140°$. Note that, as observed by Miles (1988), the inverse dependence $Z = Z(M)$ gives a possibility of multiple values of M for a given value of Z for arguments ϕ exceeding the critical value of $\phi^* = 127°$. The integration of (14) for $\phi > \phi^*$ thus demands a parametrization as suggested by Miles & Becker (1988).

The incorporation of the wavemaker dissipation renders the situation more complicated, since the function $M(Z)$ now depends on an additional parameter $a_2/\lambda_1^{\frac{1}{2}}$ also, see (15b). Even a relatively weak dissipation at the wavemaker, $a_2/\lambda_1^{\frac{1}{2}} = 0.1$, affects the shape of the function $M(Z)$ at $\phi = 173.7°$ in a notable way (cf. figure 1c). The critical value of M is now 0.293, nearly twice as large as in figure 1(a) in the absence of the wavemaker dissipation. The curve $M(Z)$ in figure 1(c) intersects itself. The functions L and K are multivalued functions of Z (cf. Miles & Becker 1988), and therefore accept different values at different passages of the intersection point. The distributions of the complex amplitude along the tank obtained from (17) for the values of M and Z corresponding to alternative approach routes to the intersection points are therefore not identical.

At $\phi = 173.7°$, $\lambda/a_1 = -10.0$ as in figure 1(c), but with a higher dissipation rate at the wavemaker, $a_2/(\lambda_1)^{\frac{1}{2}} = 0.5$, figure 1($d$), a substantially higher critical values of $M = 1.033$ below which unique stationary solutions exist, is obtained. Qualitatively, however, the shape of the curve $M = M(Z)$ remains unchanged. If the wavemaker dissipation coefficient $a_2/(\lambda_1)^{\frac{1}{2}}$ is further increased, the critical value of M below which only a single stationary solution can exist in the tank grows as well. In general, as it could be expected, incorporation of the dissipation at the wavemaker extends the range of parameters where no multiple stationary solutions are possible.

4. Relation to the experimentally meaningful parameters

4.1. *General approach*

The results of the previous section were presented as a function of three parameters: the argument of the linear coefficient in the NLS equation, ϕ, the absolute value of this coefficient, λ_1 (which is related by (15a) at the wavemaker to the parameter M), and the dissipation coefficient at the wavemaker, a_2, normalized by $\lambda_1^{\frac{1}{2}}$. Such a presentation stems naturally from the form of the equations solved, but makes it difficult to relate the conclusions directly to the experimental observations. For a given mode number n, two parameters can usually be varied at will in the experiments: the forcing amplitude, which is represented by ϵ, and the wavemaker frequency ω. In most experimental runs of BMP, KSM and Shemer & Kit (1988), the wavemaker stroke was kept constant, while the frequency was altered. In the case of purely viscous dissipation, both dissipation coefficients a_1 and a_2 depend on the forcing amplitude ϵ (Shemer & Kit 1988) and thus remain constant for a given ϵ. There is experimental evidence, however, that in reality, for a given experimental facility, the dissipation coefficient a_2 is only weakly dependent on ϵ (Shemer *et al.* 1989). For a given experimental run, the detuning coefficient λ is the only relevant parameter.

The variation of λ in the experiment corresponds to the change both in the absolute value λ_1 and in the argument ϕ of the complex linear coefficient in (6) and (9). In order to facilitate the comparison of the theoretical predictions regarding the possible stationary wave distributions in the channel, with the experimental results, the theoretical results have to be presented in terms of the physically meaningful parameters, i.e. the detuning parameter λ and the dissipation coefficients along the tank, a_1, and at the wavemaker, a_2.

4.2. *Calculational procedure*

The range of the detuning parameters λ, which we have investigated is $-10 < \lambda < 0$. This range contains the values of λ which were employed in the experiments and

where the transitions between various wave regimes were observed. Calculations were performed for three dissipation coefficients along the tank, $a_1 = 0.2$, $a_1 = 0.5$ and $a_1 = 1.0$, roughly corresponding to the estimates of the damping coefficient in various experimental conditions. For each value of the dissipation coefficient along the tank, a_1, chosen, the range of angles $\phi_{\min} < \phi < \phi_{\max}$ was selected according to (18), so that the variation of λ in the desired limits could be obtained. Equations (14) were then solved for 250 equally spaced values of ϕ within this range. For each case, the dependence $M(Z)$ was calculated according to (16) and (13) for three values of the dissipation coefficient at the wavemaker a_2: 0, 0.5 and 1.0. This selection was based on the experimental estimates of a_2 (cf. Shemer *et al.* 1989). All possible solutions of (15*a*) $Z_{0,i}$ were determined, where i denotes the running number of the root of (15*a*), and the corresponding complex amplitudes at the wavemaker $A_i(0)$ were calculated from (13) and (15*b*). These amplitudes for each value of λ_1 were then translated to the complex amplitudes of the velocity potential C_i using (9*a*). The resulting files, for each a_1 and a_2 separately, contained complex amplitudes at the wavemaker in all possible stationary states as a function of the detuning parameter λ and the solution number i and were recorded on a disk. The obtained results could thus be presented in compliance with the way in which the dependence of the experimentally obtained amplitudes on the frequency or on the amplitude is usually reported, see e.g. BMP and KSM.

4.3. *Bifurcation diagrams*

The results in the absence of dissipation at the wavemaker ($a_2 = 0$) are presented in figure 2. Both the amplitudes and the phase angles at the wavemaker are shown. For values of the detuning parameter λ that are sufficiently high, there exists a single stationary solution. When λ is decreased, a bifurcation to three possible solutions occurs. The critical value of λ at which this bifurcation is obtained decreases with increasing a_1. In the case of relatively weak damping along the tank (figure 2*a*), subsequent bifurcations to 5, 7 and 9 stationary solutions occur when λ is further decreased. There is a certain resemblance among the bifurcation diagrams at low λ for all values of a_1. Two types of solutions are obtained: a unique distribution that corresponds to a low amplitude at the wavemaker which decreases as the value of λ is lowered, and multiple regimes which have high amplitude and grow with decreasing detuning coefficient. Note that the amplitudes are very similar for all a_1 that were checked. The phase distributions presented in figure 2 indicate that all regimes which have close amplitudes are in fact quite different having phase angle which deviate significantly.

The incorporation of dissipation at the wavemaker alters the picture both quantitatively and qualitatively. At $a_2 = 0.5$ and relatively weak dissipation along the tank, $a_1 = 0.2$, figure 3(*a*), there are two distinct domains of λ where multiple stationary solutions exist. Beyond these domains, only a single stationary wave regime may exist in the tank. The dissipation at the wavemaker does not affect, however, the single possible low-amplitude regime, discussed above in the case of vanishing dissipation at the wavemaker; both the amplitudes and the phases of this regime in figure 2(*a*) are quite similar to the corresponding quantities in figure 3(*a*),

Figure 3(*b*), which represents the case with $a_2 = 0.5$ and $a_1 = 0.5$, demonstrates that the incorporation of the wavemaker dissipation may eliminate totally the existence of multiple stationary solutions. If the dissipation at the wavemaker is further decreased, a single steady solution is obtained for all λ, even when $a_1 = 0.2$. Figure 3(*c*) therefore shows a different bifurcation diagram obtained when the damping at the wavemaker is strong ($a_2 = 1.0$), but the dissipation along the tank is

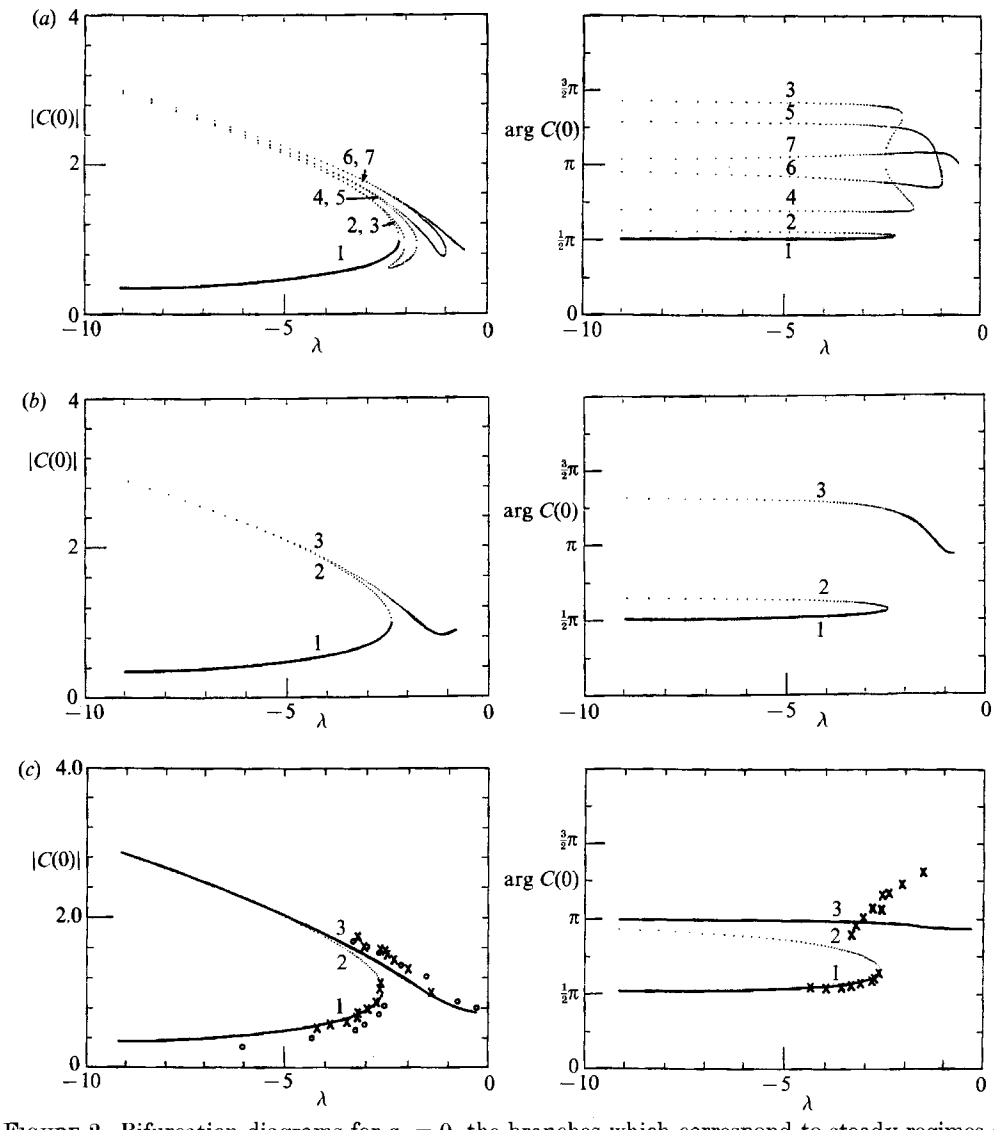

FIGURE 2. Bifurcation diagrams for $a_2 = 0$, the branches which correspond to steady regimes are drawn by a thick line. (*a*) $a_1 = 0.2$; (*b*) $a_1 = 0.5$; (*c*) $a_1 = 1.0$; o, results of BMP (their figure 5 $\epsilon = 2.47 \times 10^{-4}$); ×, results of Shemer *et al.* $\epsilon = 0.59 \times 10^{-4}$.

relatively weak, $a_1 = 0.1$. Now there is only a single relatively narrow domain where the three wave regimes are obtained.

5. Amplitude distributions along the tank

The nature of possible multiple stationary solutions is best illustrated when one plots the corresponding amplitude distribution along the tank. Figure 4 shows the profiles of the absolute values of the amplitude $C(X)$ at $a_1 = 0.2$ and $a_2 = 0$ for values of λ, which corresponds to different domains in the corresponding bifurcation diagram (figure 2*a*). The single distribution obtained for $\lambda = -0.5$, as well as most of the possible distributions at $\lambda = -2$ and at $\lambda = -3$, exhibit a strongly non

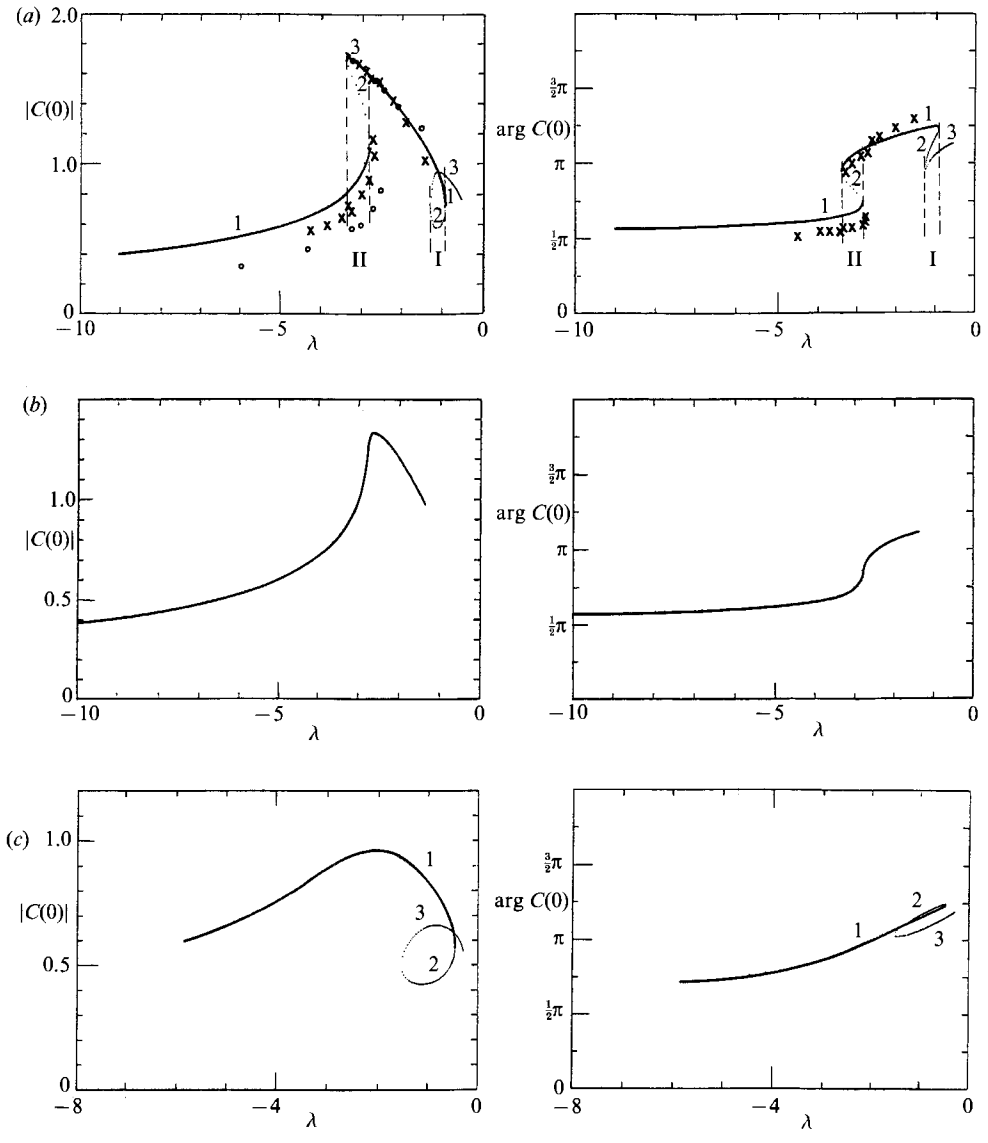

FIGURE 3. Bifurcation diagrams for $a_2 \neq 0$. (*a*) $a_1 = 0.2$, $a_2 = 0.5$; experimental points as in figure 2(*c*); (*b*) $a_1 = a_2 = 0.5$; (*c*) $a_1 = 0.1$, $a_2 = 1.0$.

monotonous shape of $|C|(X)$. Two decaying regimes labelled 1 and 2 in figure 4(*c*) are the only exceptions. The presentation in figure 4 also makes apparent the qualitative difference between the various high amplitude solutions which in figure 2(*a*) look close owing to neighbouring absolute values of the amplitude at the wavemaker.

When the dissipation along the tank is increased to $a_1 = 0.5$ in the absence of dissipation at the wavemaker, there are two possibilities: a unique solution, or three solutions (figure 2*b*). The amplitude distributions along the tank which exemplify both cases are presented in figure 5(*a*, *b*). The single solution at $\lambda = -1.0$ has a maximum at $X \neq 0$, while two of three possible stationary regimes at $\lambda = -3$ decay monotonously with X. There is no qualitative difference between the bifurcation diagram given in figure 2(*b*) and that of figure 2(*c*) for $a_1 = 1.0$, $a_2 = 0$. Stronger

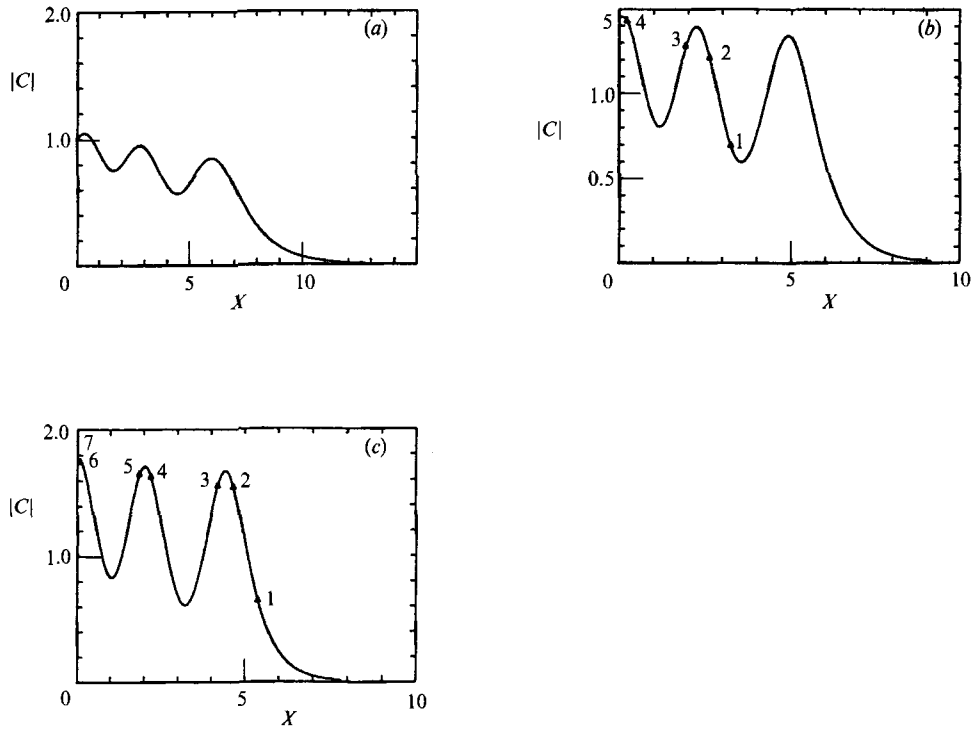

FIGURE 4. Stationary amplitude distributions along the tank, $a_1 = 0.2$, $a_2 = 0$. ▲, locations of the wavemaker which satisfy (15a); the numbers denote the corresponding branch in figure 2(a). (a) $\lambda = -0.5$; (b) $\lambda = -2.0$; (c) $\lambda = -3.0$.

dissipation along the tank, however, modifies the stationary amplitude distributions along the tank, so that only decaying regimes remain, see figure 5(c, d).

The role of dissipation at the wavemaker is now examined. The distributions along the tank which correspond to various domains in the bifurcation diagram (figure 3a) are presented in figure 6. The unique stationary regime obtained at relatively high value of $\lambda = -0.5$ (figure 6a), is quite similar to that of figure 5(a). All three possible solutions obtained at $\lambda = -1.0$ (figure 6b), have their maxima detached from the wavemaker. The single distribution at $\lambda = -2.0$, presented in figure 6(c), decays monotonously, as are all three stationary regimes in figure 6(d) at $\lambda = -3$. At lower values of λ a single monotonously decaying regime, qualitatively similar to the one shown in figure 6(c), is obtained. When the dissipation along the tank is decreased to $a_1 = 0.5$, with $a_2 = 0.5$, as in figure 3(b), the wave amplitude decays with the distance from the wavemaker for all values of the detuning coefficient λ. The distributions obtained at $a_2 = 1.0$ and $a_1 = 0.1$, corresponding to figure 3(c), do not differ qualitatively from the profiles plotted in figure 6, and for that reason they are not presented here.

6. Stability of the stationary distributions and their long-time evolution

6.1. *Background*

The results presented in the previous sections show that single stationary wave amplitude profiles exist for all λ which exceed a certain critical value. This critical

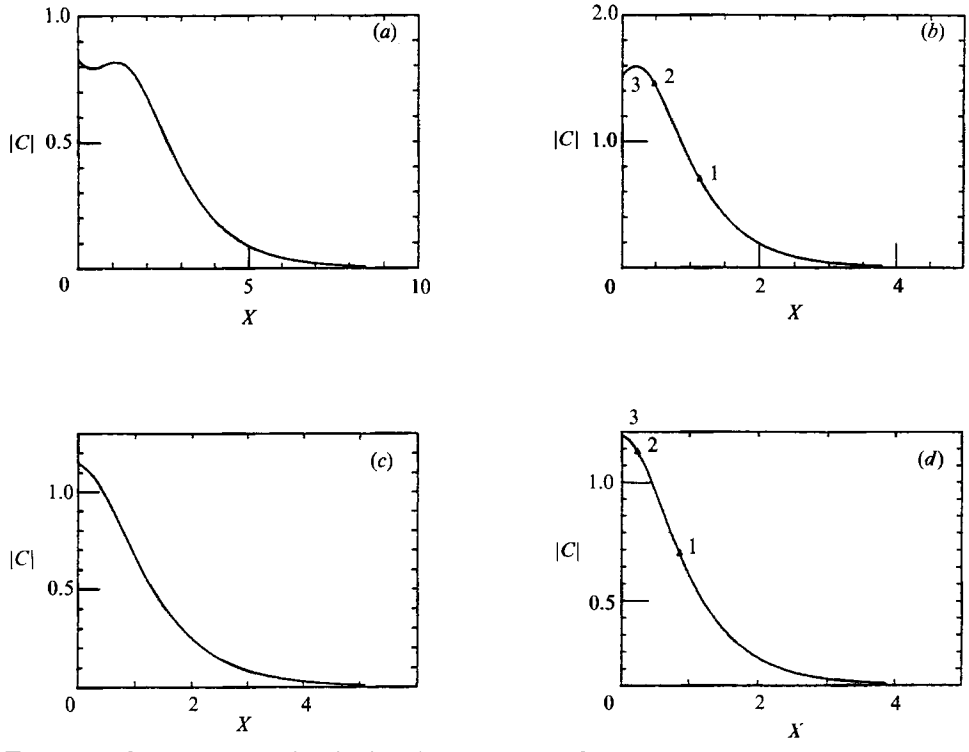

FIGURE 5. Stationary amplitude distributions along the tank, at stronger dissipation along the tank and $a_2 = 0$. Symbols as in figure 4. (*a*) $a_1 = 0.5$, $\lambda = -1.0$; (*b*) $a_1 = 0.5$, $\lambda = -3$; (*c*) $a_1 = 1.0$, $\lambda = -2.0$; (*d*) $a_1 = 1.0$, $\lambda = -3$.

value varies with a_1 and a_2 (see figures 2 and 3). At values of λ below the critical one, the bifurcation diagrams indicate a possibility of the existence of multiple stationary amplitude distributions along the tank. Miles (1988) points out that the question of stability of the stationary solutions is especially important when more than one such solution becomes possible. To the best of our knowledge, the maximum number of different wave patterns observed in various experiments at identical forcing conditions is two. BMP and Shemer *et al.* (1989) report on a possibility of two different stationary distributions, while KSM have observed in the hysteresis region either stationary or modulated (on a slow timescale) wave patterns, depending on the previous history of the wave field in the tank. Moreover, in all experiments performed in Tel-Aviv (KSM; Shemer & Kit 1988; Shemer *et al.* 1989), as well as in the numerical experiments of KSM and Shemer & Kit (1988) at λ exceeding the critical value, where a single stationary regime can exist according to figures 2 and 3, only time-modulated wave patterns were obtained. Thus, there is no direct relation between the number of stationary solutions for a given set of parameters, and the posibility of realization of these solutions, which depends on their stability.

The stability of each stationary complex amplitude distribution obtained by solving the system of equations (14)–(16) was checked by substituing such distribution as an initial condition for (5) with the boundary condition (6). The transformation of variables was performed according to (9). The NLS equation was integrated numerically using the semi-implicit Crank–Nicolson scheme. The details of the numerical procedure were given in KSM. It should be stressed here that in this way the accuracy of both the stationary solution and the NLS solver could be

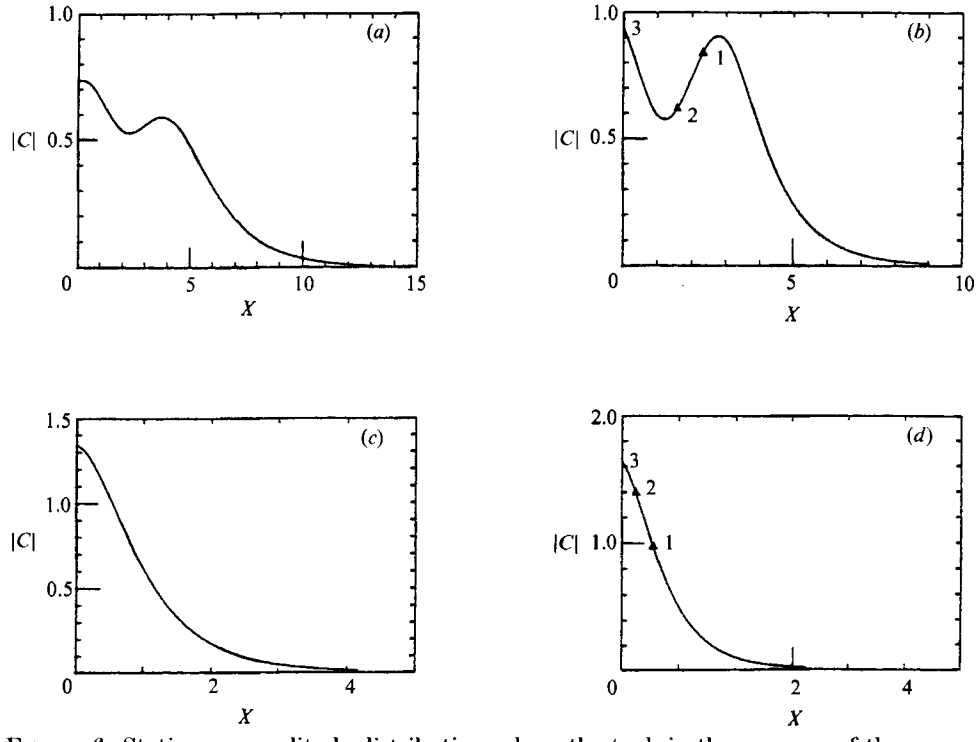

FIGURE 6. Stationary amplitude distributions along the tank in the presence of the wavemaker dissipation $a_2 = 0.5$, $a_1 = 0.2$. Symbols as in figure 4. (*a*) $\lambda = -0.5$; (*b*) $\lambda = -1.0$; (*c*) $\lambda = -2.0$; (*d*) $\lambda = -3.0$.

effectively tested. In all cases when the stationary solutions proved to be steady, the initial profile stayed essentially unchanged in time in the process of integration of the NLS equation, while the unsteady regimes remained nearly permanent only during the first stage of evolution, as long as the initial disturbance was small. It can thus be safely concluded that both the stationary and the time-dependent numerical procedures are sufficiently accurate. The time-dependent solutions obtained when the stationary distributions appear to be unstable can be presented in a visually clear manner by plotting the two-dimensional projections of the infinite-dimensional phase space, see e.g. Funakoshi & Inoue (1988). Fixed-point and limit-cycle types of solution can be clearly seen in this presentation.

6.2. *Steady regimes*

The analysis of the stability of stationary solutions shows that for all pairs of the dissipation coefficients a_1 and a_2 which correspond to single stationary distributions for the whole range of λ, e.g. $a_1 = a_1 = 0.5$ (see figure 3*b*), these stationarys profiles prove to be steady. Moreover, numerical experiments have shown that when the calculations of the time-dependent NLS equation are started with some arbitrary initial distribution, zero initial condition being a convenient example, the wave field eventually evolves to the only possible stationary distribution. Although this fact cannot serve as a conclusive proof, there are good indications that the stationary solution obtained serves as a fixed-point for an arbitrary initial condition.

Steady wave patterns alone were also obtained in the present work when $a_1 = 1.0$, $a_2 = 0$. The bifurcation diagram given in figure 2(*c*) shows that for $\lambda < -2.65$ there

are three stationary distributions. The solution of the NLS equation for λ within this range shows that two of three possible regimes are steady: the one with the minimum amplitude at the wavemaker, and the other with the maximum amplitude, labelled in figure 2(*c*) as 1 and 3, respectively. The intermediate regime 2 proves to be unsteady and is attracted to the low-amplitude distribution. The numerical experiments demonstrate a way to obtain alternative wave amplitude distributions in the tank. When the stationary solution at λ exceeding the critical value of -2.65 is substituted as an initial condition to the subsequent runs of the NLS equation with slowly decreasing values of λ, the solution is attracted to the regime represented by the upper branch in the bifurcation diagram (figure 2*c*). For increments in λ sufficiently small, it seems that it is possible to follow this branch to very low values of λ. In the present numerical experiments, λ was decreased at each run by 0.25, and the upper branch solutions were obtained until $\lambda = -17$. At this point no subsequent calculations were made. If, however, the value of λ was changed by larger steps, which in fact means that the disturbance of the stationary profile was made stronger, the solution of the time-dependent equation eventually converges to the lower branch of the bifurcation diagram. For example, when the calculations are performed at $\lambda = -9.0$ with the initial distribution corresponding to upper branch at $\lambda = -8.0$, the lower branch solution is obtained after the transients disappear. Note that when the calculations are started from zero at $\lambda < -2.65$, the stationary regime with the low amplitude at the wavemaker is eventually obtained. For $\lambda > -2.65$, any arbitrary initial condition evolves to the single possible stationary distribution along the tank.

6.3. *Modulated regimes, no wavemaker dissipation*

The substitution of the single stationary complex amplitude distribution along the tank which exists for $a_1 = 0.2$, $a_2 = 0$ and $\lambda > -1.00$ (cf. figure 4*a*) reveals that this wave regime is unsteady. In order to provide information about the time and space evolution of the wave field, the results for $\lambda = -0.5$ are presented at two cross-sections, i.e. at $X = 0$ (at the wavemaker) and at $X = 1$. The second distance was chosen as large enough so that the behaviour of the wave field away from the wavemaker is demonstrated, yet close enough to the wavemaker, so that the wave amplitudes are not negligibly small. The projections of the trajectory in the phase space starting from the stationary solution on the two-dimensional planes at $X = 0$ and $X = 1$ (figure 7*a*), indicate that a limit cycle solution is obtained. Both limit-cycles are quite similar. No stationary regimes can thus exist in the tank for the conditions corresponding to those of figure 4*a*. When the integration of the NLS equation is started from zero initial condition, the solution converges to the same limit-cycles as in figure 7(*a*). This can serve as an indication that for the chosen values of governing parameters a_1, a_2 and λ, the limit-cycle of figure 7(*a*) represents the only solution that can be realized.

The time history of $|C|$ at two points along the tank which corresponds to figure 7(*a*) is given in figure 8(*a*). The initial distribution lasts for $T \approx 5$, until the instability causes a change of the whole wave field. An organized periodical modulated pattern eventually emerges. As in figure 7(*a*), the modulation pattern is very similar at both locations shown in figure 8(*a*). The relatively well-organized character of the time evolution in figure 8(*a*) can also be seen in the power spectra of $|C|$, presented in figure 9(*a*). At both locations there is a strong peak at the frequency of modulation,with the harmonic peak being weaker by more than a decade than the main peak.

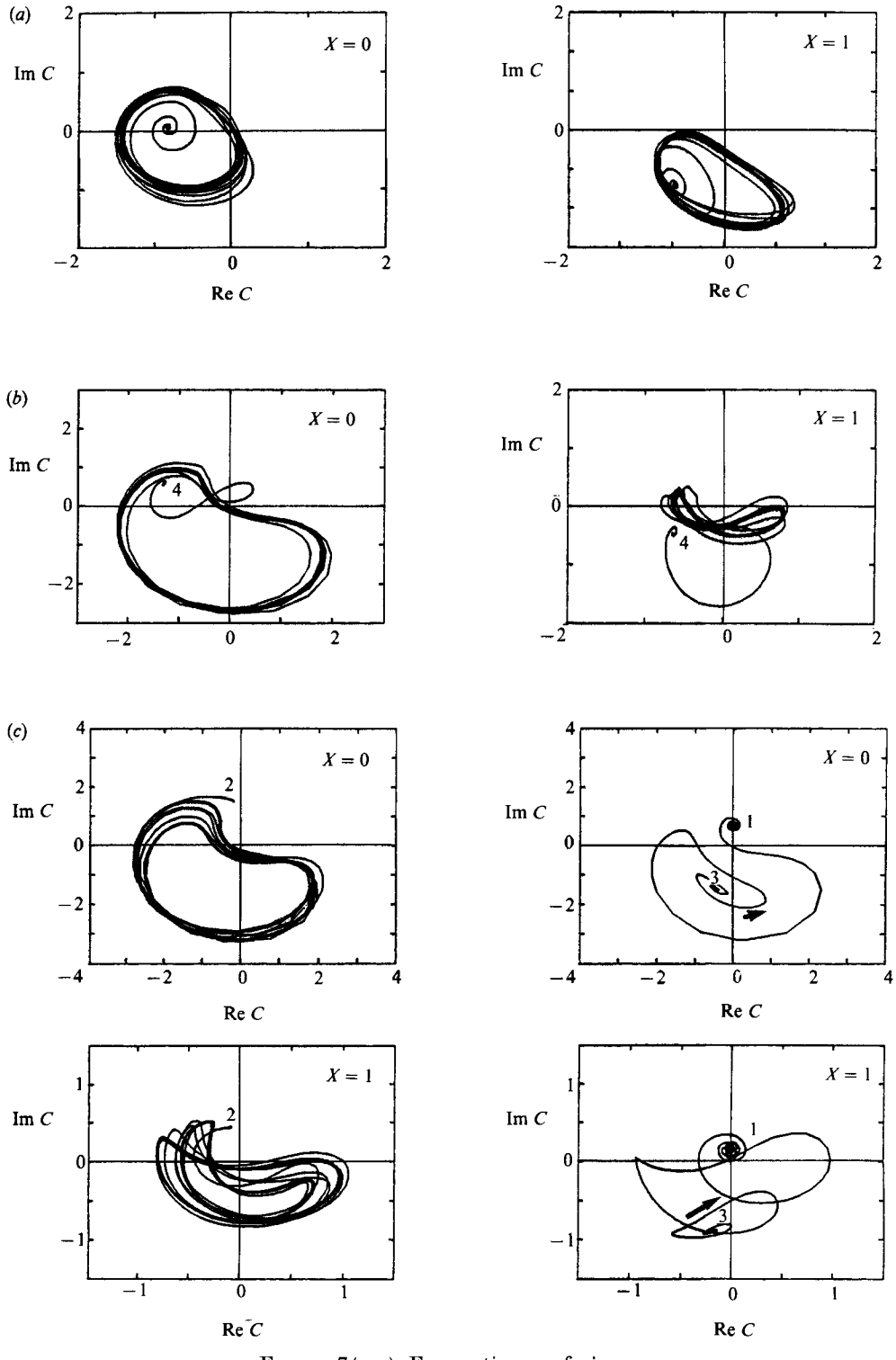

FIGURE 7(a–c). For caption see facing page.

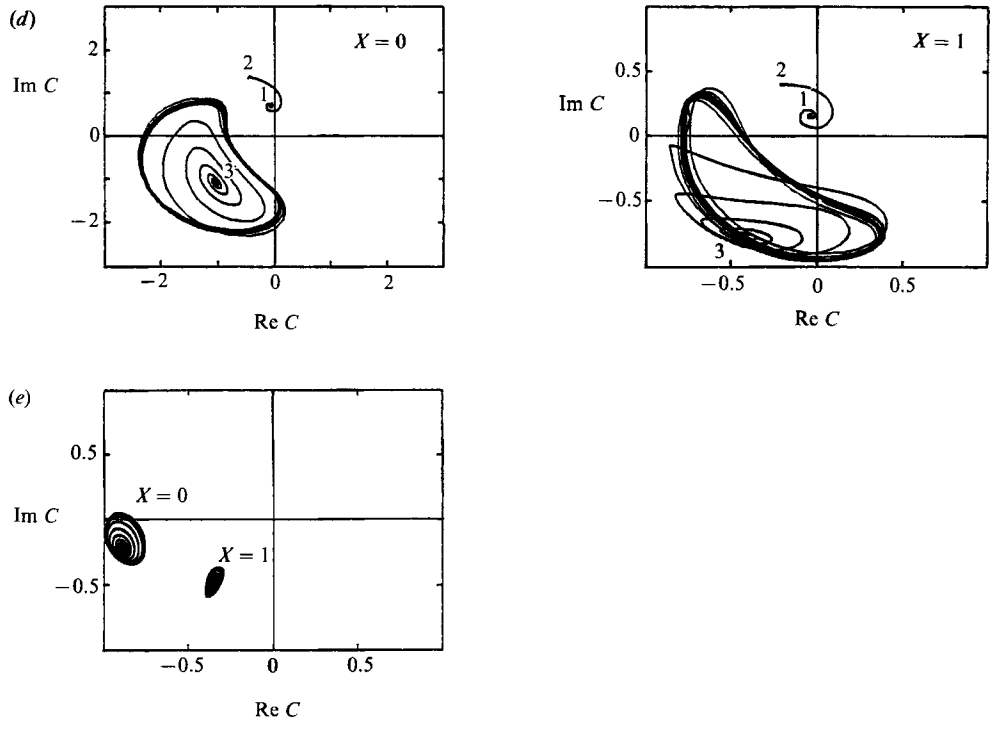

FIGURE 7. Two-dimensional projections of the trajectories in the phase space at two cross-sections. Numbers denote corresponding stationary solution in figures 2 and 3. (*a*) $a_1 = 0.2$, $a_2 = 0$, $\lambda = -0.5$; (*b*) $a_1 = 0.2$, $a_2 = 0$, $\lambda = -2.0$; (*c*) $a_1 = 0.2$, $a_2 = 0$, $\lambda = -3.0$; (*d*) $a_1 = 0.5$, $a_2 = 0$, $\lambda = -3.0$; (*e*) $a_1 = 0.2$, $a_2 = 0.5$, $\lambda = -0.9$.

Additional confirmation of the limit-cycle character and the lack of chaos in the long-time evolution of the wave field was obtained by calculating the two leading Liapunov exponents $\alpha_{1,2}$. This was done by using the approach suggested by Goldhirsch, Sulem & Orszag (1987). The complex wave amplitude $\hat{C}(X,T) = C(X,T) + \delta_j(X,T)$ is considered ($j = 1, 2$), where $C(X,T)$ is the undisturbed solution of the NLS equation (5) with the inhomogeneous boundary condition (6). The governing equation for the orthogonal disturbances $\delta_j(X,T)$ is obtained by substituting $\hat{C}(X,T)$ into (5) and (6) and linearizing the result with respect to $\delta_j(X,T)$. The resulting equation is

$$\mathrm{i}\frac{\partial \delta_j}{\partial T} + \frac{\partial^2 \delta_j}{\partial X^2} + [\lambda + a_1(1+\mathrm{i}) + 4|C(X,T)|^2]\,\delta_j + 2C^2(X,T)\,\delta_j^* = 0. \tag{19}$$

In the absence of the wavemaker dissipation, the wavemaker boundary condition for δ_j is

$$\frac{\partial \delta_j}{\partial X} = 0 \quad \text{at } X = 0. \tag{20}$$

Since (19) has coefficients which depend on T and X, it has to be solved simultaneously with (5). The Liapunov exponent α_j is defined as

$$\alpha_j = \lim_{T\to\infty} \frac{1}{T} \ln \frac{\|\delta_j(T)\|}{\|\delta_j(0)\|}, \tag{21}$$

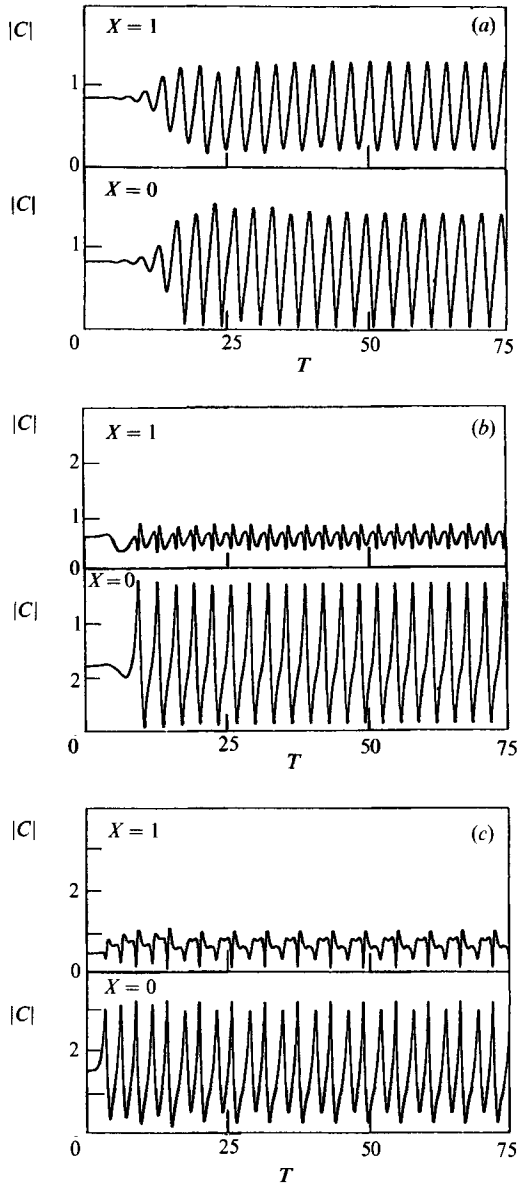

FIGURE 8. Time evolution of the unsteady stationary regimes starting from the second branch in figure 2(*a*), $a_1 = 0.2$, $a_2 = 0$, at two distances from the wavemaker. (*a*) $\lambda = -0.5$; (*b*) $\lambda = -2.0$; (*c*) $\lambda = -3.0$.

where $\|\delta_j(T)\|$ denotes the L^2 norm of δ_j. The initial distributions of $\delta_j(X)$ have to satisfy (20) and zero boundary condition at the far end of the integration domain $X_{\max}$. The second Liapunov exponent α_2 is found by periodic orthogonalization of the disturbance δ_2 relative to the most rapidly growing disturbance δ_1. Additional details regarding the calculation of the Liapunov exponents can be found in Goldhirsch *et al.* (1987).

Since three PDEs (for C, δ_1 and δ_2) have to be solved simultaneously for a long time, the calculation of $\alpha_{1,2}$ is computer-time consuming. In the present work several runs were made starting from the limit-cycle solution for $C(X, T)$ as shown in figures

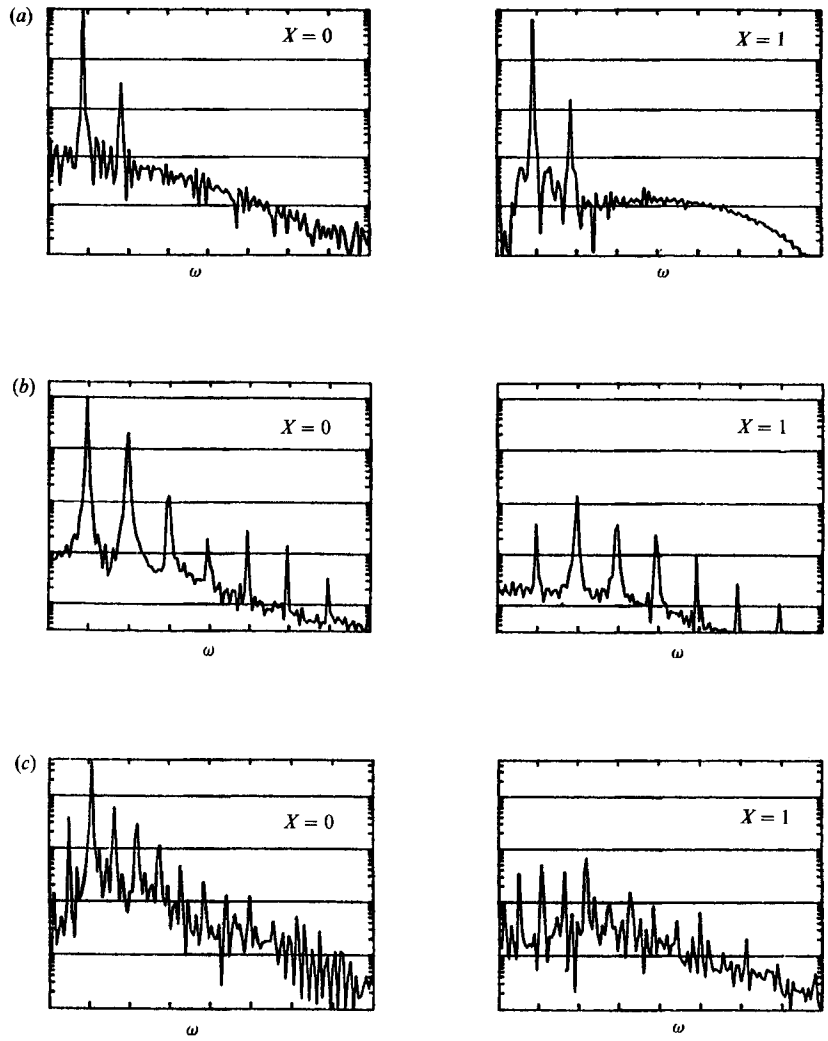

FIGURE 9. Power spectra of the absolute values of complex amplitude, the values of the amplitudes correspond to those of figure 8.

7 and 8, for a total time of $T_{\max} = 300$. The typical dependence of α on $1/T$ obtained for $a_1 = 0.2$, $a_2 = 0$ and $\lambda = -0.5$ is presented in figure 10. One can see that the asymptotic value of α_1 at $T \to \infty$ is negative and very close to zero, while $\alpha_2 < 0$. This supports the statement that the time modulation studied is non-chaotic.

The test of stability of each one of the five possible stationary distributions at $\lambda = -2$ again leads to a limit-cycle, which is the same for all five initial solutions and is presented in figure 7 (*b*). The same time-dependent solutions are obtained when the calculations are started from zero initial condition. There exists an obvious difference in the shape and in the amplitude of the cycles at $X = 0$ and $X = 1$. Examination of the time history of the wave field, which is presented for $\lambda = -2$ at figure 8 (*b*), reveals that the appearance of $|C(T)|$ at $X = 1$ is quite different from that of figure 8 (*a*). The power spectra of $|C(T)|$ given in figure 9 (*b*) show that in contrast to figure 9 (*a*), the spectra now contain numerous harmonics. The relative importance of higher harmonics in the spectrum appears to increase with the distance from the

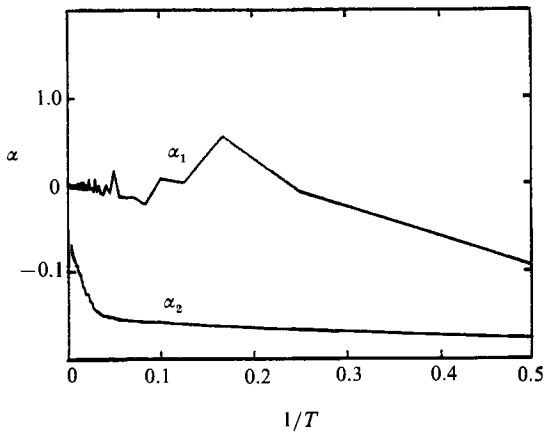

FIGURE 10. Dependence of the two leading Liapunov exponents on time, $a_2 = 0$. $a_1 = 0.2$, $\lambda = -0.5$.

wavemaker. The analysis based on the leading Liapunov exponents indicates that there is no chaos in this case as well.

Qualitative changes occur at $\lambda = -3$ (cf. figure 4*c*). In this case 7 stationary solutions exist. Two of them, labelled in figure 4(*c*) as 2 and 7, when substituted into the NLS equation as initial distributions, are attracted to the limit-cycles presented in figure 7(*c*). The rest of the possible solutions, however, take a different route and collapse to the first solution, which is a fixed-point. An identical steady solution is also obtained when integration is started from zero. An example of a fixed-point solution with the initial distribution corresponding to the branch labelled 3 in figure 4(*c*), is also presented in figure 7(*c*). Two alternative regimes can therefore be actually observed in the tank at $\lambda = -3$ for the accepted values of the dissipation coefficients: one stationary, and the other quasi-periodic. The selection of the regime is determined by the initial conditions. The analysis of figure 7(*c*) shows that these limit-cycles exhibit period doubling. The time history of the corresponding wave amplitudes is presented in figure 8(*c*). The spectra of figure 9(*c*) reveal that the addition of the low-frequency component affects the whole spectrum, and the number of peaks grows substantially.

When the detuning coefficient is further decreased to $\lambda = -5$, there are five possible stationary solutions, all of which are attracted to the single steady regime which corresponds to the lowest amplitude branch in the bifurcation diagram and decays monotonously along the tank. If, however, the calculations at $\lambda = -5$ are started with the initial condition corresponding to the limit-cycle distribution at $\lambda = -3$ at an arbitrary time, the limit-cycle solution is obtained. The modulated regime can be sustained by gradually reducing the detuning coefficient to $\lambda = -10.0$, where the stationary solution corresponding to the upper amplitude branch is obtained for all initial conditions.

The branch labelled 1 on the bifurcation diagram (figure 2*a*) is thus the only branch which gives a steady solution for all λ. This branch corresponds to stationary distributions with the shortest region of substantially non-zero wave amplitudes (cf. figure 4*c*). In most cases, the wave amplitude at the wavemaker for this branch is also minimal among all possible stationary solutions. The single exception is in the range $-2.49 < \lambda < -2.21$, where two out of nine possible stationary distributions have a lower amplitude at the wavemaker than that of branch 1. The numerical runs

performed in this range confirm the stability of the regime corresponding to branch 1, while all other stationary distributions evolve to a limit-cycle.

The present numerical experiments thus indicate that for $a_1 = 0.2$ and $a_2 = 0$, a single limit-cycle type of solution is obtained for $\lambda > -2.21$, one steady and one modulated in time wave regime can be obtained for $-10 < \lambda < -2.21$, while for extremely low values of λ two stationary regimes, which correspond to the extreme branches on the amplitude diagram (figure 2*a*), appear to be stable.

Somewhat similar results are obtained at $a_1 = 0.5$ (figure 2*b*). The main difference with the previous case is that now the single possible stationary distribution, which corresponds to the branch labelled 3 in figure 2(*b*), is stable for $\lambda = -1$ (the corresponding amplitude distribution along the tank is given in figure 5*a*). When this branch is followed to lower values of the detuning parameter λ, the stationary distribution gradually becomes unstable and evolves to a limit-cycle. At $\lambda = -3$, the rate of growth of instability of the stationary solution is extremely low, the amplitude of modulation is small, so that the time-dependent regime still does not deviate notably from the stationary solution. The range of variation of $|C(T)|$ increases notably when λ is reduced. The limit-cycle obtained at $\lambda = -3$ is presented in figure 7(*d*). The pattern of variation of the absolute value of the wave amplitude with time is quite similar to that of figure 8(*a*). The distribution labelled 1 in figure 5(*b*) at $\lambda = -3$, is stable, and the intermediate stationary solution converges to this stable solution. At lower values of λ this limit-cycle seems to disappear and the upper branch solution at $\lambda = -10$ is stable.

6.4. *Modulated regimes*, $a_2 \neq 0$

The bifurcation diagram for $a_1 = 0.2$ and $a_2 = 0.5$ (figure 3*a*), suggests that there are two domains of λ where three stationary solutions are possible, whereas beyond these domains only unique stationary solutions exist. The stability check reveals that at high values of the detuning coefficient, $\lambda > -0.94$, where the unique stationary solution exists, the situation is similar to that in the corresponding domain for $a_1 = 0.5$, $a_2 = 0$. The stationary regimes are unstable, but the modulated solutions deviate only slightly from the stationary profiles. An example of the limit cycle obtained just beyond the first domain of triple solutions, $\lambda = -0.9$, is plotted at figure 7(*e*). Note that the limit cycle of figure 7(*e*) is plotted for a total duration of $T = 150$, in contrast to $T < 75$ in the rest of figure 7. This duration was necessary owing to the slow growth rate of instability of the stationary solution. The transient effects disappear in this case only after the duration of computations exceeds $T = 100$. Out of three possible distributions at $-1.28 < \lambda < -0.94$, shown in figure 6(*b*) for $\lambda = -1.0$, only the regime labelled by 1 is steady, while any other initial condition checked, including the distributions labelled 2 and 3, eventually evolves to this only possible steady solution.

The branch corresponding to the steady distribution in the first domain of the multivalued solutions is the only one which is continued in the bifurcation diagram (figure 3*a*) when λ is reduced. Unique stationary profiles obtained at $-2.84 < \lambda < -1.28$ are steady. The solution labelled 3 in the second domain of triple solutions, $-3.37 < \lambda < -2.84$, also corresponds to the same branch and is stable. As usual, the distribution labelled 1 in figure 6(*d*) is stable, while the intermediate solution 2 is attracted to the first one. Hysteresis between two stationary solutions is thus obtained for $-3.37 < \lambda < -2.84$. It is interesting to note that the basin of attraction of the fixed point corresponding to the first solutions in this domain seems to be substantially larger than that of the third solution. Most arbitrary initial

distributions checked in the numerical experiments, including the initially undisturbed water surface, evolve to the first profile. The third solution, however, appears to be stable to certain finite disturbances. For example, when the stationary profile labelled 3 in figure 6(*d*) is multiplied by a factor 1.1, the disturbed distribution returns to the undisturbed profile.

At $a_1 = 0.1$, $a_2 = 1.0$ (figure 3*d*), the stability pattern is similar to that of figure 3(*a*). At the values of the detuning coefficient exceeding the domain of triple solutions, stationary profiles are unsteady and an arbitrary initial distribution evolves to a modulation of limit cycle type. The branch labelled by 1 in figure 3(*c*) corresponds to steady solutions for all $\lambda < -0.47$. The other stationary distributions, as well as other initial conditions checked, are attracted to this steady distribution, which thus serves as the only fixed point.

7. Comparison with the experimental data

Detailed measurements of directly excited stationary resonant standing waves were reported by BMP and Shemer *et al.* (1989). Quantitative comparison of the theoretical results with these experiments requires, however, exact knowledge of both complex dissipation coefficients, $\hat{a}_1$ and $\hat{a}_2$. As mentioned above, the theoretically obtained coefficients seem to be below their actual values (Shemer & Kit 1988). For that reason, for any given facility both $\hat{a}_1$ and $\hat{a}_2$ have to be evaluated by comparing the model predictions with the measured data. BMP have disregarded the dissipation at the wavemaker, and estimated the absolute value of a_1 in their tank (translated to our variables) to be in the range $1.96 \times 10^{-4} < a_1 \epsilon < 3.63 \times 10^{-4}$. The correspondence between the parameters of BMP and ours can be established by the procedure used by Miles (1988). For the highest forcing amplitude employed in the BMP experiments (their $\epsilon = 0.046$, corresponding to our $\epsilon = 2.47 \times 10^{-4}$), they observed, in a certain range of forcing frequencies, two different wave amplitudes in the tank (see their figure 5). As can be seen from figure 2, in the absence of wavemaker dissipation, multiple stationary wave regimes can only be obtained when $a_1 > 0.5$. The value of the dissipation coefficient along the tank, as estimated by BMP for that forcing amplitude, is $0.8 < a_1 < 1.47$. The dissipation coefficient $a_1 = 1.0$ (figure 2*c*) is therefore within this range.

The rescaled wave amplitudes measured by BMP in the vicinity of the wavemaker at $\epsilon = 2.47 \times 10^{-4}$ are plotted in figure 2(*c*). The quantitative agreement between the experimental data and the theoretical curves seems reasonable. The model also provides the correct value of $\lambda = -2.7$ where the transition from the lower to the upper branch occurs. However, as discussed in §6.2, the upper branch in figure 2(*c*) extends to very low values of λ, while in the experiments the reverse transition to the lower branch was observed for $\lambda < -3.4$.

The experimental data obtained by Shemer *et al.* (1989) for $\epsilon = 0.59 \times 10^{-4}$ are also presented in figure 2(*c*) for comparison. There is a remarkably good agreement between the results acquired in entirely different facilities. Here again, the model appears to represent correctly the absolute values of the wave amplitude, as well as the transitional value of the detuning coefficient (the 'jump' from low to high amplitudes occurs in these experiments at $\lambda = -2.66$). The reverse transition to lower amplitudes takes place at $\lambda = -3.25$, giving an extent of the hysteresis domain similar to that observed by BMP. The inability of the theory to describe this reverse transition and the finite range of λ where the hysteresis is obtained represents thus

essential deficiency of the model which does not take into account the wavemaker dissipation.

The wave phases reported by Shemer *et al.* (1989) are plotted in figure 2(*c*) as well. The agreement of their experimental data obtained in the low-amplitude regime with the theoretical curve labelled 1 is very good. However, the qualitative behaviour of $\arg C(0)$ in the regime which corresponds to branch 3 appears to be quite different from the model prediction. As noticed already by BMP, the phase measurements provide a sensitive tool for assessing the correctness of the theoretical model. Hence, both the lack of the reverse transition and the phase behaviour of the model indicate that the reasonable agreement between the measured wave amplitudes and the theoretical curves may be fortuitous.

There is every reason to believe that the theoretical value of a_1, which is obtained by taking into account only a purely viscous dissipation mechanism, yields the correct order of magnitude of the dissipation coefficient at smooth walls (Shemer & Kit 1988). When calculated for both BMP and Shemer *et al.* (1989) experimental conditions, the dissipation coefficient along the tank appears to be lower by an order of magnitude than $a_1 = 1.0$ accepted in figure 2(*c*). On the other hand, direct experimental estimates of the dissipation coefficient at the wavemaker by Shemer *et al.* give $a_2 = O(1)$. This is in general agreement with the values chosen by Shemer & Kit (1988) based on comparison of the numerical solutions of the NLS equation with the experimental results. The amplitudes and phases measured by BMP and Shemer *et al.* were therefore also plotted in figure 3(*a*) ($a_1 = 0.2$, $a_2 = 0.5$), since these values of both dissipation coefficients seem to be more realistic. Both sets of experimental data comply well with the theoretical curves. The two major shortcomings of the model with vanishing dissipation at the wavemaker have now been removed. The region of hysteresis predicted by the model is in agreement with the experimental results, and the variation of the wave phase with λ obtained in the experiment follows the theoretical curves.

Moreover, the incorporation of the wavemaker dissipation in the theoretical model describes the transition to the modulated regime, as well. The transition value of $\lambda - 0.94$ (cf. §6.4), is in a good agreement with the corresponding experimental values of $\lambda = -0.57$ and $\lambda = -1.24$, reported by KSM and Shemer & Kit (1988) for two modifications of the wavemaker geometry.

It should be stressed here that incorporation of the wavemaker dissipation in the model by simple modification of the boundary condition at $X = 0$ according to (6) and (7), does not take into account complicated mechanisms like vortex shedding at the wavemaker, owing to its discontinuities. It is reasonable to assume that such mechanisms contribute significantly to the wavemaker dissipation (Shemer & Kit 1988). However, even this simplified model allows us to reproduce correctly all major features of the wave field.

8. Discusion and concluding remarks

In the present investigation the problem of the directly excited resonant standing waves in a tank is considered following the general approach suggested by Miles (1988). All possible stationary solutions for any given set of the experimental parameters are found first. The bifurcation diagrams given in figures 2 and 3 delineate the boundaries between the qualitatively different domains and thus provide guidelines for the subsequent analysis of the unsteady wave fields. The results of §6 demonstrate that the bifurcation of the steady solutions is closely

related to the transition between the wave regimes in the tank. The bifurcations diagrams show that numerous stationary solutions can be obtained, especially in the case with vanishing dissipation at the wavemaker. The results of the present numerical study, however, indicate that not more than two different wave regimes can exist in the tank. This is in agreement with the available experimental data.

The close relation between the bifurcation diagrams and the transition between different wave regimes, as observed in experiments and obtained numerically, can be understood by examining the structure of these diagrams. The branch on the bifurcation diagram which corresponds to the most easily achieved steady distribution at low values of the detuning parameter λ, comes from $-\infty$ and ends at some critical λ (cf. figures 2, 3). An increase in λ beyond this critical value therefore necessarily requires the existence of a sharp transition to an alternative wave regime. The alternative regime can be either steady, and thus correspond to an another branch in the diagram, or modulated on a slow timescale. If this alternative solution can be preserved when λ is decreased below its critical value, hysteresis is obtained.

KSM, and in particular Shemer & Kit (1988) stressed the importance of the incorporation of the dissipation at the wavemaker in order to obtain agreement between the numerical and the experimental results. By selecting a proper value of the complex dissipation coefficient at the wavemaker, Shemer & Kit managed to obtain good quantitative agreement between the theory and the experiment for the whole range of the experimental parameters. They have failed, however, to reproduce numerically the hysteresis which was observed in the experiments. The present results reveal the reason for that failure. Relatively small variations in the values of the dissipation coefficients can significantly alter the general shape of the bifurcation diagrams. Hysteresis in finite ranges of the detuning coefficients λ can only be expected when 'loops' appear in the bifurcation diagrams. The approach adopted in the present study provides an overall view of the problem, based on the bifurcation diagrams, and thus clearly shows the regions of possible hysteresis for any given set of parameters. The important conclusion of the present study is that these 'loops' can only exist when the wavemaker dissipation is taken into account. The close relation between finite domains of hysteresis, on one hand, and incorporation of dissipation in the wavemaker boundary condition, on the other hand, is thus established.

Both steady and limit-cycle solutions were obtained. For certain values of the damping coefficients, there is a domain of λ where these two regimes can be found at identical forcing conditions. The possibility of obtaining numerically the hysteresis of the kind observed in the experiments is thus demonstrated. In other experiments, two different steady distributions were obtained in the tank. This type of hysteresis is also obtained in the present investigation for sufficiently high damping rates along the tank.

The question about the possibility of chaotic modulation in the directly generated resonant waves in a tank remains open. The experimental evidence on this aspect of the problem cannot be decisive owing to the extremely long duration of the experiment that seems to be necessary to make meaningful conclusions possible. The approach adopted in the present study can, in principle, provide a numerical answer for a given experimental situation, i.e. for given values of the damping coefficients. Such an endeavour demands a systematic scanning of all relevant parameters and thus requires a considerable effort and large computing times.

The author wishes to thank his colleagues E. Kit and I. Goldhirsch for valuable discussions, numerous suggestions and criticism.

REFERENCES

BARNARD, B. J. S., MAHONY, J. J. & PRITCHARD, W. G. 1977 The excitation of surface waves near a cut-off frequency. *Phil. Trans. R. Soc. Lond.* A **286**, 87–123.

CILIBERTO, S. & GOLLUB, J. P. 1985 Chaotic mode competition in parametrically forced surface waves. *J. Fluid Mech.* **158**, 381–398.

FUNAKOSHI, M. & INOUE, S. 1988 Surface waves due to resonant horizontal oscillation. *J. Fluid Mech.* **192**, 219–247.

GOLDHIRSCH, I., SULEM, P.-L. & ORSZAG, S. A. 1987 Stability and Liapunov stability of dynamical systems: a differential approach and a numerical method. *Physica* **27D**, 311–337.

KIT, E. & SHEMER, L. 1989 On the neutral stability of cross-waves. *Phys. Fluids* A **1**, 128–1132.

KIT, E., SHEMER, L. & MILOH, T. 1987 Experimental and theoretical investigation of nonlinear sloshing waves in a rectangular channel. *J. Fluid Mech.* **181**, 265–291.

MILES, J. 1988 Guided surface waves near cutoff. *J. Fluid Mech.* **189**, 287–300.

MILES, J. & BECKER, J. 1988 Parametrically excited, progressive cross-waves. *J. Fluid Mech.* **186**, 129–146.

SHEMER, L., CHEMESSE, M. & KIT, E. 1989 Measurements of the dissipation coefficient at the wavemaker in the process of generation of the resonant standing waves in a tank. *Exp. Fluids* **7**, 506–512.

SHEMER, L. & KIT, E. 1988 Study of the role of dissipation in evolution of nonlinear sloshing waves in a rectangular channel. *Fluid Dyn. Res.* **4**, 89–105.

UMEKI, M. & KAMBE, T. 1989 Nonlinear dynamics and chaos in parametrically excited surface waves. *J. Phys. Soc. Japan* **58**, 140–154.